Draft version September 5, 2018
Typeset using LaTeX **twocolumn** style in AASTeX62

Search for an intrinsic metallicity spread in old globular clusters of the Large Magellanic Cloud

Andrés E. Piatti[1,2] and Andreas Koch[3]

[1] *Consejo Nacional de Investigaciones Científicas y Técnicas, Av. Rivadavia 1917, C1033AAJ, Buenos Aires, Argentina*
[2] *Observatorio Astronómico de Córdoba, Laprida 854, 5000, Córdoba, Argentina*
[3] *Zentrum für Astronomie der Universität Heidelberg, Astronomisches Rechen-Institut, Mönchhofstr. 12, 69120 Heidelberg, Germany*

ABSTRACT

We report for the first time on the magnitude of the intrinsic [Fe/H] spread among ten old globular clusters (GCs) of the Large Magellanic Cloud (LMC). Such spreads are merely observed in approximately five per cent of the Milky Way GCs and recently gained more attention in theoretical models of GC evolution. We derived metallicities with a typical precision of 0.05 dex $\leq \sigma$[Fe/H] $\leq$ 0.20 dex for an average of 14 red giant branch stars per GC from Strömgren photometry. The respective, metallicity-sensitive indices have been calibrated to precise and accurate high-dispersion spectroscopy. For all clusters we found null [Fe/H] spreads with a typical uncertainty of 0.04 dex, with the possible exception of NGC 1786 that shows an intrinsic dispersion of 0.07$\pm$0.04 dex. The mean, observed standard deviation of the derived metallicities for nearly 40 per cent of our GC sample amounted to smaller than 0.05 dex. At present, we cannot exclude that the remaining GCs also have intrinsic Fe-abundance variations in excess of 0.05 dex, but in order to significantly detect those, the measurement errors on individual [Fe/H]-values would need to be lowered to the 0.03–0.07 dex level. These findings suggest, along with those from ages and light-element abundances, that the LMC GCs studied here are alike to the majority of Galactic GCs.

Keywords: techniques: photometric — galaxies: individual (LMC) — galaxies: star clusters: general — globular clusters: general

1. INTRODUCTION

Only 8 out of 156 Galactic globular clusters (GCs) listed in the (Harris 1996, 2010 version) catalog have been recently classified as 'anomalous' objects, because their intrinsic [Fe/H] dispersions are $>$ 0.05 dex (Johnson et al. 2015; Marino et al. 2015). From this perspective, anomalies in the iron content would not appear to be the most frequent manifestation of the GC multiple populations (MPs) formation, as recently reviewed by Bastian & Lardo (2017).

Among the 15 known Large Magellanic Cloud (LMC) old GCs, only NGC 1754, 2210, and 2257 have been searched for anomalies in their metallicities by Mucciarelli et al. (2009), who concluded from [Fe/H] values of 5–7 stars per GC that they exhibit quite homogeneous iron abundances (intrinsic spread=0.02–0.04 dex) despite the observed occurrence of light element variations such as an Na-O anti-correlation. Therefore, they show very similar properties to the vast majority of Galactic GCs.

From a theoretical point of view, different models have recently proposed distinct scenarios to describe abundance anomalies in a variety of chemical elements in massive clusters harboring MPs. For instance, Bekki & Tsujimoto (2016)'s model is based on merger events, Bekki (2017) and Kim & Lee (2018) used supernovae enrichment and asymptotic giant branch (AGB) star ejecta, while Gieles et al. (2018) proposed a concurrent formation of GCs and supermassive stars, among others. These models have been mainly stimulated by observational findings of (anti-)correlations between chemical abundances of certain light elements (e.g., Na-O, Mg-Al, Mg-Si, Si-Zn; Osborn 1971; Cohen 1978; Carretta et al. 2009; Gratton et al. 2012; Hanke et al. 2017) and bimodalities in CN and CH that trace light element variations (e.g. Kayser et al. 2008; Martell & Grebel 2010, and references therein). Some of the models also propose mechanisms to obtain intrinsic [Fe/H] spreads $>$ 0.05 dex. For instance, Gavagnin et al. (2016)'s model

Corresponding author: Andrés E. Piatti
e-mail: andres@oac.unc.edu.ar

used merger events, while that of Bailin (2018) is based on feedback from core-collapse supernovae. Recently, Lim et al. (2017) found that GCs with large intrinsic [Fe/H] spreads also show a positive CN-CH correlation.

In this work we report on the magnitude of the intrinsic [Fe/H] spread for a sample of nine old LMC GCs and in ESO 121-SC03, which lies in the LMC's GC age gap (9 Gyr, Bica et al. 1998; Mackey et al. 2006). As far as we are aware, this is the largest sample of LMC GCs – assumed to have MPs but not confirmed as yet – analyzed in order to search for internal metallicity variations. In Section 2 we describe the observational material and precision and accuracy of our photometry. Section 3 deals with the estimation of individual metallicities for carefully selected cluster red giant branch (RGB) stars, while in Section 4 we analyze and discuss our results.

2. OBSERVATIONAL DATA SETS

We made use of publicly available images of ten LMC GCs obtained through the Strömgren *vby* filters with the SOAR Optical Imager (SOI) mounted on the 4.1-m Southern Astrophysical Research (SOAR) telescope (program SO2008B-0917, PI: G. Pietrzyński). The images (field of view = $5.25' \times 5.25'$, pixel scale = $0.154''$/px) were obtained from exposures of 350–500, 140–300 and 90–180 s in the v, b, and y filters, respectively, under excellent atmospheric conditions (FWHM $\sim 0.6''$). We processed the images, along with the respective calibration images, following the SOI pipeline[1].

Stellar photometry on the individual images was obtained using the DAOPHOT package (Stetson et al. 1990). We first derived a quadratically varying point-spread-function (PSF) by using two sets of stars selected interactively, one with ∼100 and another with the brightest ∼40 stars. The smaller group was used to build a preliminary PSF, which was in turn used to clean the larger PSF sample. The resulting PSF was applied to all the identified stars in an image, which were then subtracted from it in order to identify fainter stars, and to run again ALLSTAR on the enlarged star sample. We iterated the loop three times. Finally, we kept only sources with $\chi < 2$, |SHARPNESS| < 0.5, and DAOPHOT photometric errors smaller than 0.01 mag.

To standardize the PSF photometry we first measured instrumental magnitudes of 5–10 standard stars observed twice per night, thus covering an airmass range between 1.1 and 2.1. Then, we fitted the transformation equations given by the expressions:

$$v = v_1 + V_{\rm std} + v_2 \times X_v + v_3 \times (b-y)_{\rm std} + v_4 \times m_{\rm 1std},$$
$$b = b_1 + V_{\rm std} + b_2 \times X_b + b_3 \times (b-y)_{\rm std},$$
$$y = y_1 + V_{\rm std} + y_2 \times X_y + y_3 \times (b-y)_{\rm std},$$

where v_i, b_i and y_i are the i-th fitted coefficients, and X represents the effective airmass. Table 1 shows the resulting coefficients obtained using the IRAF.FITPARAMS routine.

The quality of our photometry was first examined in order to obtain robust estimates of the photometric errors. To do this, we performed artificial star tests by using the stand-alone ADDSTAR program in the DAOPHOT package (Stetson et al. 1990) to add synthetic stars, generated bearing in mind the color and magnitude distributions of the stars in the color-magnitude diagram (CMD) as well as the cluster radial stellar density profile. We added a number of stars equivalent to $\sim 5\%$ of the measured stars in order to avoid in the synthetic images significantly more crowding than in the original images. On the other hand, to avoid small number statistics in the artificial-star analysis, we created a thousand different images for each original one. We used the option of entering the number of photons per ADU in order to properly add the Poisson noise to the star images.

We then repeated the same steps to obtain the photometry of the synthetic images as described above, i.e., performing three passes with the DAOPHOT/ALLSTAR routines. The photometric errors were derived from the magnitude difference between the output and input data of the added synthetic stars using the DAOMATCH and DAOMASTER tasks. We found that this difference resulted typically equal to zero and in all the cases smaller than 0.003 mag. The respective rms errors were adopted as the photometric errors. Fig. 1 illustrates the behavior of these errors as a function of the distance from the cluster center and of the magnitude. For clarity, we only show two different magnitude level, namely $V =$ 16.5 mag and 18.5 mag, respectively. These magnitudes roughly correspond to the upper and lower limits of the cluster RGBs used in this work (see Fig. 2).

3. METALLICITY ESTIMATES

We used the m_1 vs. $b-y$, m_1 vs. $v-y$, V vs. $b-y$, and V vs. $v-y$ diagrams as discriminators between giant, subgiant, and dwarf stars (thus weeding out foreground stars) to select RGB stars in stellar populations (Faria 2007; Arnadottir 2010; Calamida et al. 2012, 2014). We contrained our search to RGB stars located inside the cluster radii estimated by Piatti & Mackey (2018), and brighter that the respective cluster horizontal branch

[1] http://www.ctio.noao.edu/soar/content/soar-optical-imager-soi

Table 1. Strömgren transformation coefficients.

Filter	coef$_1$	coef$_2$	coef$_3$	coef$_4$	rms
Dec. 18, 2008: NGC 2257, ESO 121-SC3					
v	1.122±0.007	0.295±0.005	1.995±0.048	1.026±0.061	0.002
b	0.942±0.014	0.177±0.009	0.946±0.014	...	0.008
y	0.932±0.015	0.122±0.009	-0.005±0.016	...	0.010
Dec. 19, 2008: NGC 1754, 1786, 1835, 1898, 2005, 2019, 2210					
v	1.096±0.015	0.286±0.009	2.004±0.030	1.117±0.038	0.010
b	0.916±0.013	0.169±0.007	0.999±0.011	...	0.010
y	0.939±0.019	0.107±0.010	0.018±0.015	...	0.016
Jan. 16, 2009: NGC 1841					
v	1.005±0.004	0.290±0.009	2.034±0.032	0.914±0.028	0.007
b	1.014±0.007	0.170±0.007	0.939±0.018	...	0.011
y	1.005±0.004	0.120±0.010	-0.046±0.011	...	0.007

in the V vs. $b-y$ CMD, where the RGBs are narrower and least contaminated by field stars (Frank et al. 2015). Indeed, we only kept stars within a strip of ±0.05 mag in $b-y$ from the cluster RGB ridge lines, assumed the $b-y$ color to be mainly a temperature effective indicator with less metallicity sensitivity (Crawford & Mandwewala 1976). We also discarded any star lying inside the RGB strips whose [Fe/H] value departs significantly (more than 3 times the observed dispersion) from the readily visible cluster metallicity distributions. In addition, by using different field regions of equal cluster areas, distributed around the clusters, we found that the number of field stars which fall inside the RGB strips is smaller than 10 per cent with respect to the total number of adopted cluster members. Fig. 2 shows all the measured stars inside the cluster radius, those located far from the cluster region for an equal cluster area, and the selected RGB stars drawn with black, orange and red filled circles, respectively.

By using the semi-empirical calibration by Calamida et al. (2007), we estimated individual metallicities ([Fe/H]) from the reddening corrected metallicity index[2] m_{10}, in turn based on the stars' $(v-y)_0$ colors. The uncertaintes were calculated from propagation of all of the involved errors, i.e., those of the calibration and those of our photometry, as follows:

$$m_{10} = \alpha + \beta[\mathrm{Fe/H}] + \gamma(v-y)_0 + \delta[\mathrm{Fe/H}](v-y)_0,$$

where $\alpha = -0.309$, β=−0.090±0.002, γ=0.521±0.001, and δ=0.159±0.001, respectively. Then, per standard error propagation,

$$\begin{aligned}\sigma([\mathrm{Fe/H}])^2 &= \left(\frac{\partial[\mathrm{Fe/H}]}{\partial\alpha}\sigma(\alpha)\right)^2 + \left(\frac{\partial[\mathrm{Fe/H}]}{\partial\beta}\sigma(\beta)\right)^2 \\ &+ \left(\frac{\partial[\mathrm{Fe/H}]}{\partial\gamma}\sigma(\gamma)\right)^2 + \left(\frac{\partial[\mathrm{Fe/H}]}{\partial\delta}\sigma(\delta)\right)^2 \\ &+ \left(\frac{\partial[\mathrm{Fe/H}]}{\partial m_{10}}\sigma(m_{10})\right)^2 + \left(\frac{\partial[\mathrm{Fe/H}]}{\partial(v-y)_0}\sigma((v-y)_0)\right)^2 \\ &= \left(\frac{0.002[\mathrm{Fe/H}]}{c}\right)^2 + \left(\frac{0.001(v-y)_0}{c}\right)^2 \\ &+ \left(\frac{0.001[\mathrm{Fe/H}](v-y)_0}{c}\right)^2 + \left(\frac{\sigma(m_{10})}{c}\right)^2 \\ &+ \left(\frac{(-0.521c - 0.159(m_{10} + 0.309 - 0.521(v-y)_0)\sigma((v-y)_0)}{c^2}\right)^2,\end{aligned}$$

where c = −0.090+0.159$(v-y)_0$, and $\sigma(m_{10})$ and $\sigma((v-y)_0)$ are the photometric errors in m_{10} and $(v-y)_0$, respectively, according to the position of the stars with respect to the cluster's center (see Fig. 1). We note that m_{10} and $(v-y)_0$ depend on the vby magnitudes of each star, in the sense that the fainter a star, the larger its errors. They also depend on the position of the star respect to the cluster center, because of crowding effects. Typically, stars located in the outer regions have smaller magnitude errors as compared with those of the same magnitudes placed at the cluster center. We derived them as follows:

$$\begin{aligned}(v-y)_0 &= v - y - 1.67 \times 0.74E(B-V), \\ \sigma((v-y)_0)^2 &= \sigma(v)^2 + \sigma(y)^2 + (1.67 \times 0.74\sigma(E(B-V)))^2\end{aligned}$$

and

$$m_{10} = (v-b) - (b-y) + 0.33 \times 0.74E(B-V),$$

[2] Using the standard definition $m_1 = (v-b) - (b-y)$.

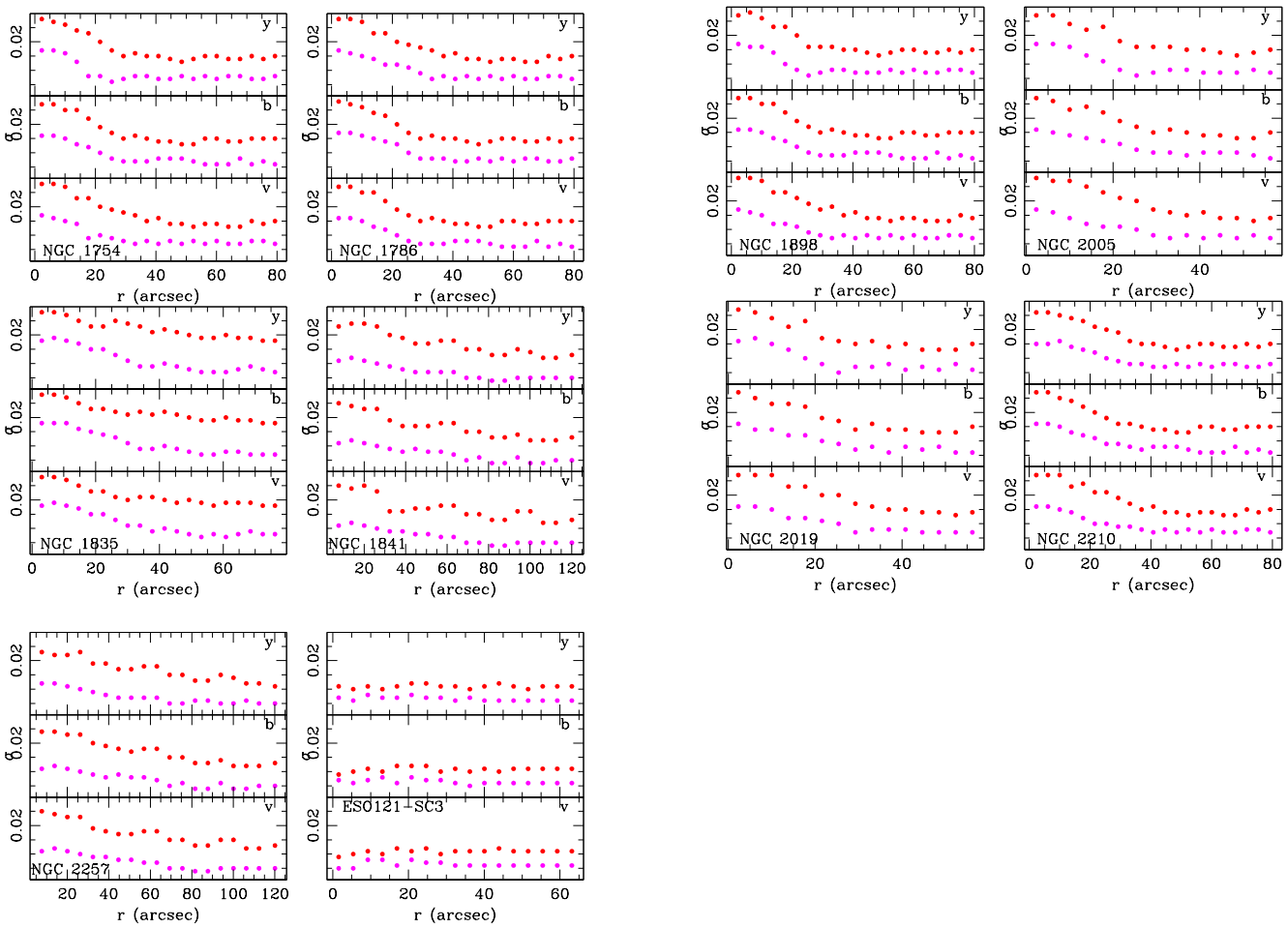

Figure 1. Photometric error estimates for the *vby* filters as a function of the distance to the cluster center. Magenta and red filled circles are for $V = 16.5$ and 18.5 mag, respectively.

$$\sigma(m_{10})^2 = \sigma(v)^2 + 4\sigma(b)^2 + \sigma(y)^2 + (0.33 \times 0.74\sigma(E(B-V)))^2,$$

where the reddening laws, $E(X)/E(B-V)$, are those given by Crawford & Mandwewala (1976). We obtained the cluster reddening values from the NASA/IPAC Extragalactic Data base[3] (NED) (see Table 2). The resulting [Fe/H] values and their errors are plotted in the bottom-right panels of Fig. 2.

3.1. *Intrinsic dispersions*

We next determined the mean and dispersion of each cluster's Fe-abundance by employing a maximum likelihood approach, similar to the method detailed in Frank et al. (2015). The relevance lies in accounting for each individual star's measurement errors, which could artificially inflate the dispersion if ignored. We optimized the probability $\mathcal{L}$ that a given ensemble of stars with metallicities $[\mathrm{Fe/H}]_i$ and metallicity errors σ_i are drawn from a population with mean Fe-abundance <[Fe/H]> and intrinsic dispersion W (e.g., Walker et al. 2006; Koch et al. 2018), as follows:

$$\mathcal{L} = \prod_{i=1}^{N} \left(2\pi \left[\sigma_i^2 + W^2\right]\right)^{-\frac{1}{2}} \times \exp\left(-\frac{([\mathrm{Fe/H}]_i - <[\mathrm{Fe/H}]>)^2}{\sigma_i^2 + W^2}\right),$$

where the errors on the mean and dispersion were computed from the respective covariance matrices. We note that this approach assumes that the error distribution is Gaussian, which is adopted here because of the limited number of stars (cf. Frank et al. 2015). The last columns of Table 2 list the mean metallicity, the intrinsic dispersion, and the number of stars used for each cluster. As far as we are aware, these comprise the largest sample of LMC GCs with metallicities put on an homogeneous

[3] http://ned.ipac.caltech.edu/. NED is operated by the Jet Propulsion Laboratory, California Institute of Technology, under contract with NASA.

scale. Here, we note the remarkably tight correlation between the spectroscopic and Strömgren-based metallicities, attesting to the validity of the calibrations over a broad metallicity- and color-range (see Fig. 3). Moreover, although the CN absorption band at λ4142Å is near to the effective wavelength of the v filter, our metallicities appear to be also driven by Fe abundances, as the index m_1 was calibrated by Calamida et al. (2007) as a photometric proxy for the iron abundance. Nevertheless, we cannot rule out that they could also reflect CN variations (Lim et al. 2017).

3.2. *Foreground contamination*

Our measured intrinsic dispersions values are not expected to be affected by field star contamination, since the LMC field stellar population have more metal-rich mean metallicities (e.g., Cole et al. 2000; Pompéia et al. 2008; Carrera et al. 2011; Van der Swaelmen et al. 2013; Piatti & Geisler 2013), and Milky Way (MW) stars placed along the cluster RGB sequences are expected to be negligible across the relative small cluster areas ($r \lesssim 1.5'$ Piatti & Mackey 2018).

We show in the σ[Fe/H] vs. [Fe/H] plots of Fig. 2 every measured field star located in the observed cluster areas, and distributed outside the adopted cluster RGB strips (black circles). For comparison we also included field stars from regions outside the cluster areas (orange circles). As can be seen, these do not visibly widen the metallicity range of the selected stars. We note that field RGB stars younger than the GCs have [Fe/H] > -1.0 dex (Cole et al. 2005; Piatti & Geisler 2013) and are placed along GC RGBs with [Fe/H] > -1.0 dex, depending on their ages (Geisler et al. 2003; Ordoñez & Sarajedini 2015).

In order to assess the influence of LMC field star contaminants on our measurements, we expanded the above likelihood estimator by adding a fraction f of foreground stars (Koch et al. 2007):

$$\begin{aligned}\mathcal{L} = \prod_{i=1}^{N} (1-f) \ \left(2\pi \ \left[(\sigma_i^2 + W^2\right]\right)^{-\frac{1}{2}} \\ \times \quad \exp\left(-\frac{([\mathrm{Fe/H}]_i - <[\mathrm{Fe/H}]>)^2}{\sigma_i^2 + W^2}\right), \\ + \quad f\, p([\mathrm{Fe/H}])\end{aligned}$$

Here, the metallicity distribution function p([Fe/H]) of the contaminants was drawn from the observed Strömgren-metallicity distribution of LMC field stars of Cole et al. (2000). This was done exemplary for NGC 1786, the only object in our sample that shows a hint of a significant intrinsic spread. As a result, even fractions as high as >90% will leave the result significant at the 1σ-level.

Secondly, we removed stars from the NGC 1786 sample at random in a jackknife manner, recomputing the mean and dispersion as before. As a result, even upon rejection of three stars (amounting to 20% of the entire sample) as if they were foreground contaminants, did not alter the measured, non-negligible intrinsic dispersion and maintained the significance of the result. As for the other GCs with null dispersions, their results also remained unaffected, yielding the low-to-zeros values as before.

3.3. *AGB star contamination*

Stellar populations such as GCs in the MW and the LMC can be expected to host a non-zero population of AGB stars, which can add a contamination of up to 10% of stellar samples as analysed here (e.g. Kamath et al. 2010). This is exemplified in ESO 121-SC3 (bottom panel of Fig. 2), which has six *bona fide* members in the analysis. The scatter in metallicity appears dominated by a single object yielding a low metallicity. As the brightest star observed in the cluster, near the tip of the RGB we cannot refute that this star is a potentially variable star on the AGB, rather than an RGB star.

To assess their influence on the metallicity spreads, we first consulted a set of Padova isochrones (Bressan et al. 2012), available in the Stömgren system, with ages and metallicities tailored to the individual GCs of this study. We then created random samples of stars matching the observed numbers. and designed them to lie either on the theoretical RGB or AGB tracks; next, we computed their metallicities from the above calibrations, using the isochrone's $(v-y)$ and m_1 colors. Albeit the isochrones', per construction, mono-metallicity, this procedure already introduced a standard deviation on the order of 0.04 dex from this theoretical consideration for either class of stars. Moreover, metallicities derived from AGB stars are on average lower by merely 0.02 dex, so that the inclusion of a minor contamination (1–2 stars per GC) in our, presumed RGB samples, would not lead to a significant inflation of the intrinsic dispersion if they were misclassified as RGB stars.

However, we note that, as being warmer and less massive than RGB stars, metallicities of AGB stars should follow different relations of the Calamida et al. (2007) calibration that used here, also due to the different strength of the molecular bands, with weaker CN- and CH-bands. Ideally, the AGB contamination should be weeded out by using the index $c_1 = (u-v) - (v-b)$ that is sensitive to stellar evolutionary stage (Arnadottir 2010), but this is inhibited by the lack of any u-band observations for our LMC targets.

4. ANALYSIS AND DISCUSSION

The resulting dispersions reveal that nine of the ten LMC GCs studied here show metallicity spreads consistent with zero within the respective errors, as it is the case for most of the MW GCs. One possible exception is NGC 1786, at $W = 0.07 \pm 0.04$ dex. The posteriori likelihood distribution for its mean metallicity and intrinsic dispersion is shown in Fig. 4. We note that all our results include a thorough consideration of all errors propagated through the calibration for each star, giving a realistic account of the, non-necessarily symmetric, error distribution.

In order to obtain W values larger than 0.05 dex, errors of the individual metallicities of our selected stars would need to be smaller than 0.04 dex (NGC 1754), 0.10 dex (NGC 1786), 0.03 dex (NGC 1835), 0.07 dex (NGC 1841), 0.03 dex (NGC 1898), and 0.06 dex (NGC 2005), respectively. For the remaining GCs the standard deviation of the derived [Fe/H] values is smaller than 0.05 dex, so that we discarded those GCs as possible candidates for Fe-abundance anomalies. They represent 40 per cent of the whole analyzed sample. The estimated upper limits in the [Fe/H] uncertainties put a demanding constraint on the precision of [Fe/H] estimates. Indeed, by using only NGC 1786's stars with a tighter error constraint σ[Fe/H] < 0.10 dex, we derived W = 0.07±0.04 dex (N=8). For other GCs we did not reach the expected metallicity uncertainties, which could be attempted to be obtained from high S/N, high-dispersion spectroscopy.

As far as we are aware, there is no study showing the existence of MPs among the LMC's old GC population from their color-magnitude diagrams (cf. Milone et al. 2009), although three of them display the give-away light element abundance signatures such as a Na-O anticorrelation. In fact, as equivalents of MW GCs, they are assumed to harbor MPs, and there is an acceptable synchronicity between their ages (Wagner-Kaiser et al. 2017) and the abundances of some light chemical elements (Mucciarelli et al. 2010), and overlap of their mass and age to relaxation-time ratio ranges (Piatti & Mackey 2018). As the [Fe/H]-spread is concerned, the eight MW GCs with Fe-abundance variations larger than 0.05 dex represent nearly five per cent of the whole GC population. If such a small percentage were applicable to the LMC GC population, we should find no more than one GC with such a metallicity spread, in agreement with our findings for NGC 1786 (at a significance of $\sim 1.7\sigma$).

This work represent the first attempt in measuring the iron abundance variation in most of the LMC GCs so far. We were motivated by the fact that Fe-abundance variations are found among some MW GCs and by the increasing number of theoretical models that predict the presence of such chemical inhomogeneities. We used on average 14 selected RGB stars per cluster and obtained [Fe/H] values with uncertainties smaller than 0.20 dex, and nearly comparable accuracy to that derived from high-dispersion spectroscopy for some of the brightest stars. We tightly reproduced their generally accepted spectroscopic metallicity scale and found no hint – except for NGC 1786 – for a metallicity spread. This outcome supports that LMC GCs share chemical abundance patterns similar to those seen in many of their Galactic counterparts, as has been suggested from the comparative, high-resolution abundance measurements in the LMC GCs (Mucciarelli et al. 2010; Bastian & Lardo 2017).

Based on observations obtained at the Southern Astrophysical Research (SOAR) telescope, which is a joint project of the Ministério da Ciência, Tecnologia, Inovações e Comunicações (MCTIC) do Brasil, the U.S. National Optical Astronomy Observatory (NOAO), the University of North Carolina at Chapel Hill (UNC), and Michigan State University (MSU). AK gratefully acknowledges support from the German Research Foundation (DFG) via Sonderforschungsbereich SFB 881 ('The Milky Way System', subproject A08). We thank C.I. Johnson and A. Mucciarelli for useful comments. We thank the referee for the thorough reading of the manuscript and timely suggestions to improve it.

REFERENCES

Árnadóttir, A. S., Feltzing, S., & Lundström, I. 2010, A&A, 521, A40

Bailin, J. 2018, ArXiv e-prints. https://arxiv.org/abs/1807.01447

Bastian, N., & Lardo, C. 2017, ArXiv e-prints. https://arxiv.org/abs/1712.01286

Beasley, M. A., Hoyle, F., & Sharples, R. M. 2002, MNRAS, 336, 168, doi: 10.1046/j.1365-8711.2002.05714.x

Bekki, K. 2017, MNRAS, 469, 2933, doi: 10.1093/mnras/stx982

Bekki, K., & Tsujimoto, T. 2016, ApJ, 831, 70, doi: 10.3847/0004-637X/831/1/70

Bica, E., Geisler, D., Dottori, H., et al. 1998, AJ, 116, 723, doi: 10.1086/300448

Bressan, A., Marigo, P., Girardi, L., et al. 2012, MNRAS, 427, 127

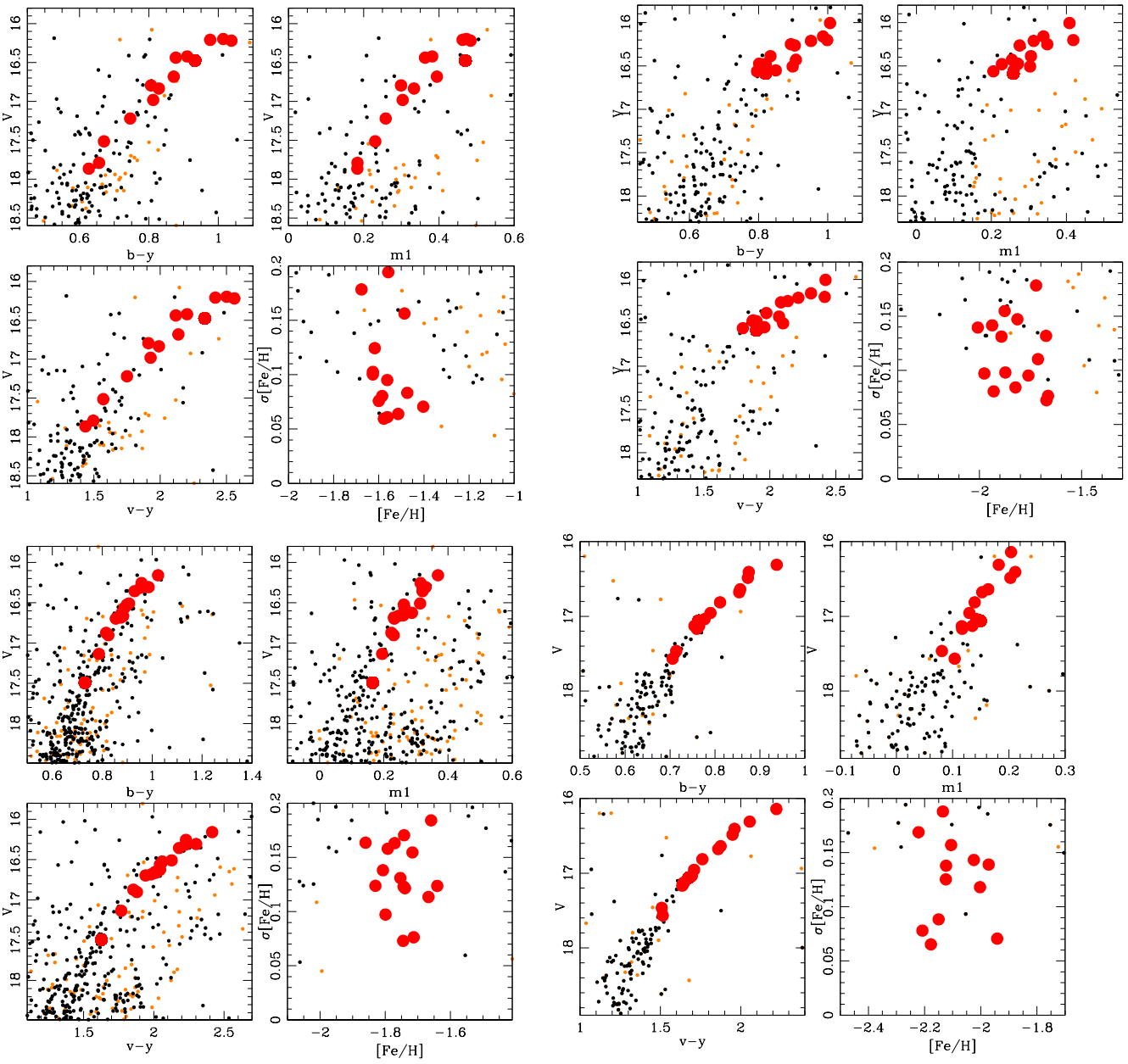

Figure 2. CMDs of stars observed in the field of the GCs NGC 1754 (top-left), NGC 1786 (top-right), NGC 1835 (bottom-left), and NGC 1841 (bottom-right). Black and orange filled circles represent stars observed in the cluster area and in a comparison star field with an equal cluster area, respectively. Selected stars are drawn with larger red circles. The individual metallicities ([Fe/H]) and their respective uncertainties are depicted in the bottom-right panel. respectively.

Calamida, A., Monelli, M., Milone, A. P., et al. 2012, A&A, 544, A152, doi: 10.1051/0004-6361/201219712

Calamida, A., Bono, G., Stetson, P. B., et al. 2007, ApJ, 670, 400, doi: 10.1086/521424

Calamida, A., Bono, G., Lagioia, E. P., et al. 2014, A&A, 565, A8, doi: 10.1051/0004-6361/201323081

Carretta, E., Bragaglia, A., Gratton, R., & Lucatello, S. 2009, A&A, 505, 139, doi: 10.1051/0004-6361/200912097

Carrera, R., Gallart, C., Aparicio, A., & Hardy, E. 2011, AJ, 142, 61

Cohen, J. G. 1978, ApJ, 223, 487, doi: 10.1086/156284

Cole, A. A., Smecker-Hane, T. A., & Gallagher, J. S., III 2000, AJ, 120, 1808

Cole, A. A., Tolstoy, E., Gallagher, III, J. S., & Smecker-Hane, T. A. 2005, AJ, 129, 1465, doi: 10.1086/428007

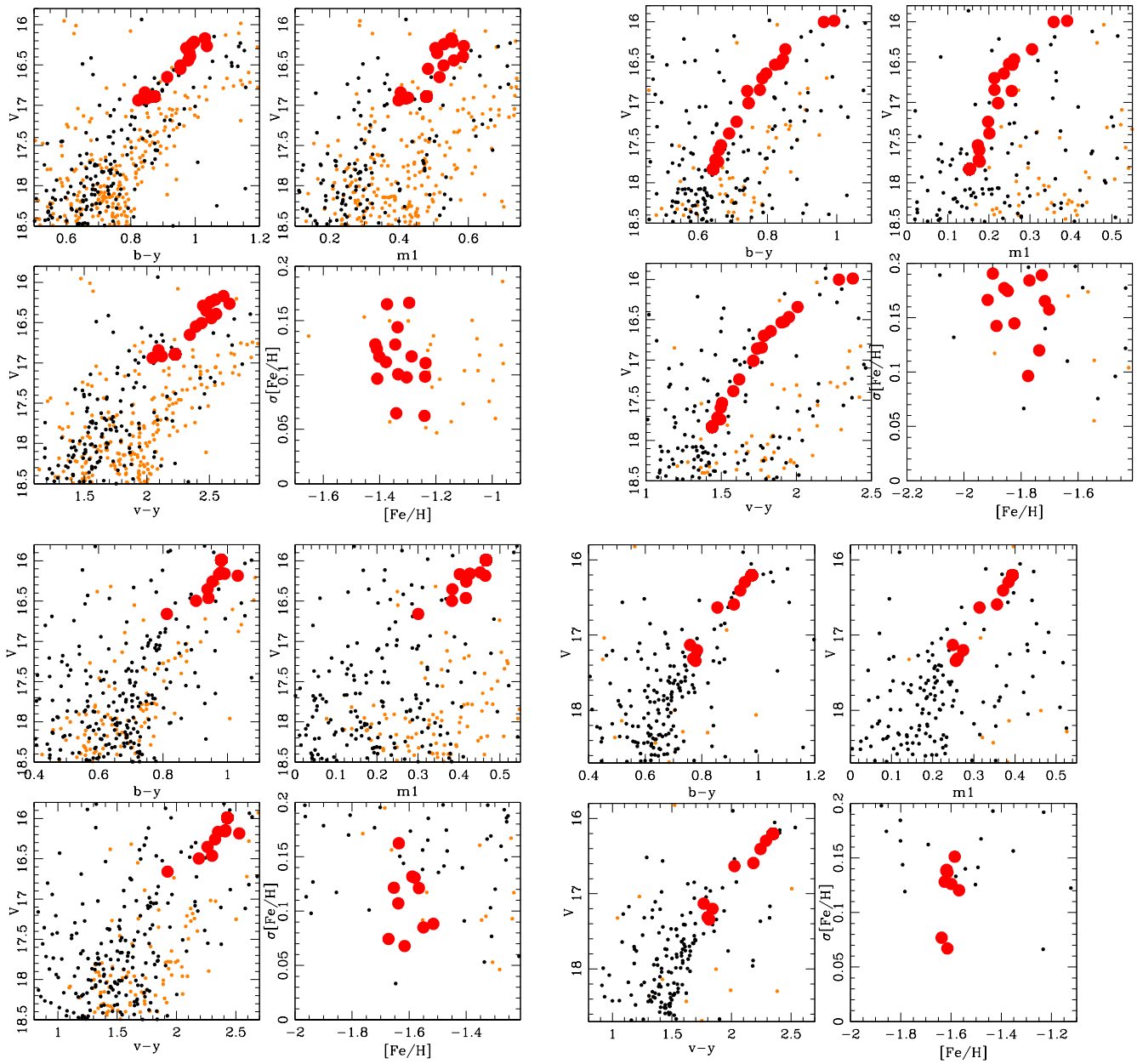

Figure 2. (continued). NGC 1898 (top-left), NGC 2005 (top-right), NGC 2019 (bottom-left), and NGC 2210 (bottom-right).

Crawford, D. L., & Mandwewala, N. 1976, PASP, 88, 917, doi: 10.1086/130046

Faria, D., Feltzing, S., Lundström, I., et al. 2007, A&A, 465, 357

Frank, M. J., Koch, A., Feltzing, S., et al. 2015, A&A, 581, A72, doi: 10.1051/0004-6361/201526555

Gavagnin, E., Mapelli, M., & Lake, G. 2016, MNRAS, 461, 1276, doi: 10.1093/mnras/stw1397

Geisler, D., Piatti, A. E., Bica, E., & Clariá, J. J. 2003, MNRAS, 341, 771, doi: 10.1046/j.1365-8711.2003.06408.x

Gieles, M., Charbonnel, C., Krause, M. G. H., et al. 2018, MNRAS, 478, 2461, doi: 10.1093/mnras/sty1059

Gratton, R. G., Carretta, E., & Bragaglia, A. 2012, A&A Rv, 20, 50, doi: 10.1007/s00159-012-0050-3

Hanke, M., Koch, A., Hansen, C. J., & McWilliam, A. 2017, A&A, 599, A97, doi: 10.1051/0004-6361/201629650

Harris, W. E. 1996, AJ, 112, 1487, doi: 10.1086/118116

Haschke, R., Grebel, E. K., Frebel, A., et al. 2012, AJ, 144, 88

Johnson, C. I., Rich, R. M., Pilachowski, C. A., et al. 2015, AJ, 150, 63, doi: 10.1088/0004-6256/150/2/63

Johnson, J. A., Ivans, I. I., & Stetson, P. B. 2006, ApJ, 640, 801, doi: 10.1086/498882

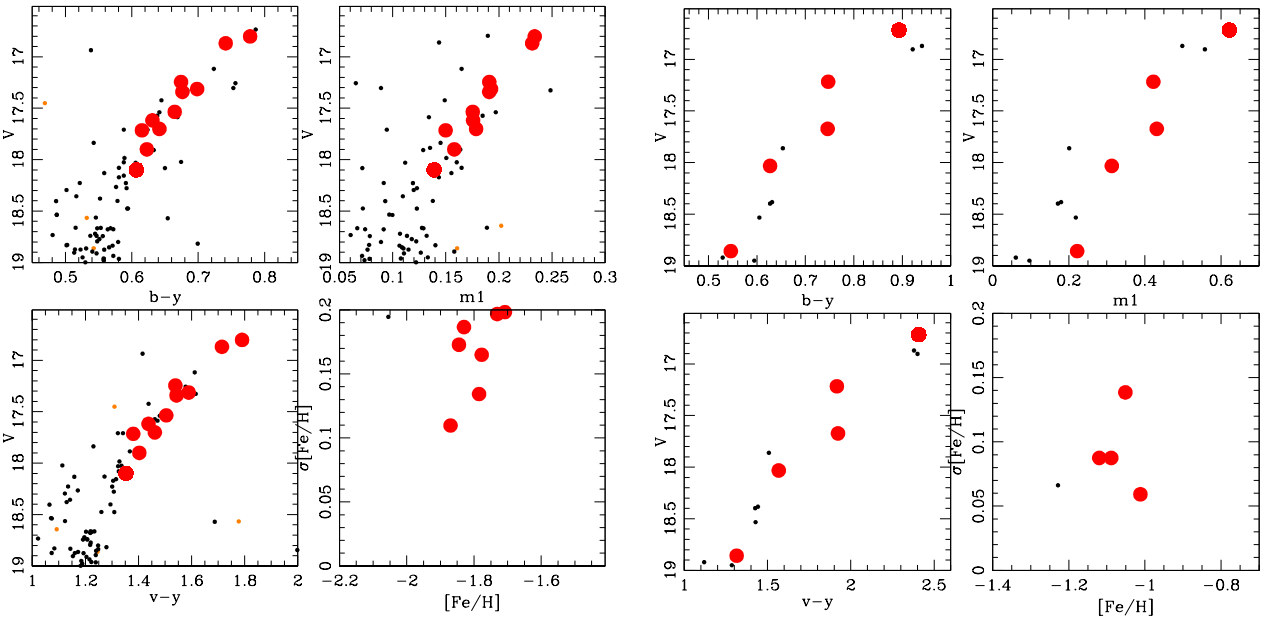

Figure 2. (continued). NGC 2257 (left), and ESO 121-SC3 (riggt).

Table 2. Astrophysical properties of LMC GCs

ID	E(B-V)$_{NED}$[a]	Age	Ref.	[Fe/H]	Ref.	<[Fe/H]>	W	N
	(mag)	(Gyr)		(dex)		(dex)	(dex)	
NGC 1754	0.07	12.96	2	-1.50±0.10	4,5	-1.54±0.02	0.00±0.05	14
NGC 1786	0.07	12.30	7	-1.75±0.10	1,4,5	-1.80±0.03	0.05±0.03	15
NGC 1835	0.14	13.37	2	-1.72±0.10	4,5	-1.74±0.03	0.00±0.03	16
NGC 1841	0.14	12.57	2	-2.02±0.10	4	-2.10±0.03	0.00±0.02	15
NGC 1898	0.07	13.50	7	-1.32±0.10	4,5,6	-1.32±0.02	0.00±0.03	16
NGC 2005	0.07	13.77	2	-1.74±0.10	4,5,6	-1.32±0.02	0.00±0.03	16
NGC 2019	0.07	16.20	2	-1.56±0.10	4,5,6	-1.79±0.04	0.00±0.05	18
NGC 2210	0.10	10.43	2	-1.55±0.10	1,2	-1.61±0.02	0.00±0.04	9
NGC 2257	0.05	11.54	2	-1.77±0.10	1,4,2	-1.80±0.05	0.00±0.06	11
ESO 121-SC3	0.04	8.50	7	-1.05±0.20	3	-1.05±0.04	0.00±0.05	5

NOTE—[a] Errors taken from the standard deviation of $E(B-V)$ values of the selected stars are < 0.01 mag.
Ref.: (1) Mucciarelli et al. (2009); (2) Wagner-Kaiser et al. (2018); (3) Bica et al. (1998); (4) Suntzeff et al. (1992); (5) Beasley et al. (2002); (6) Johnson et al. (2006); (7) Piatti et al. (2009).

Kamath, D., Wood, P. R., Soszyński, I., & Lebzelter, T. 2010, MNRAS, 408, 522

Kayser, A., Hilker, M., Grebel, E. K., & Willemsen, P. G. 2008, A&A, 486, 437, doi: 10.1051/0004-6361:200809446

Kim, J. J., & Lee, Y.-W. 2018, ArXiv e-prints. https://arxiv.org/abs/1807.01317

Koch, A., Wilkinson, M. I., Kleyna, J. T., et al. 2007, ApJ, 657, 241

Koch, A., Hansen, T. T., & Kunder, A. 2018, A&A, 609, A13, doi: 10.1051/0004-6361/201731434

Lim, D., Hong, S., & Lee, Y.-W. 2017, ApJ, 844, 14, doi: 10.3847/1538-4357/aa79aa

Mackey, A. D., Payne, M. J., & Gilmore, G. F. 2006, MNRAS, 369, 921

Marino, A. F., Milone, A. P., Karakas, A. I., et al. 2015, MNRAS, 450, 815, doi: 10.1093/mnras/stv420

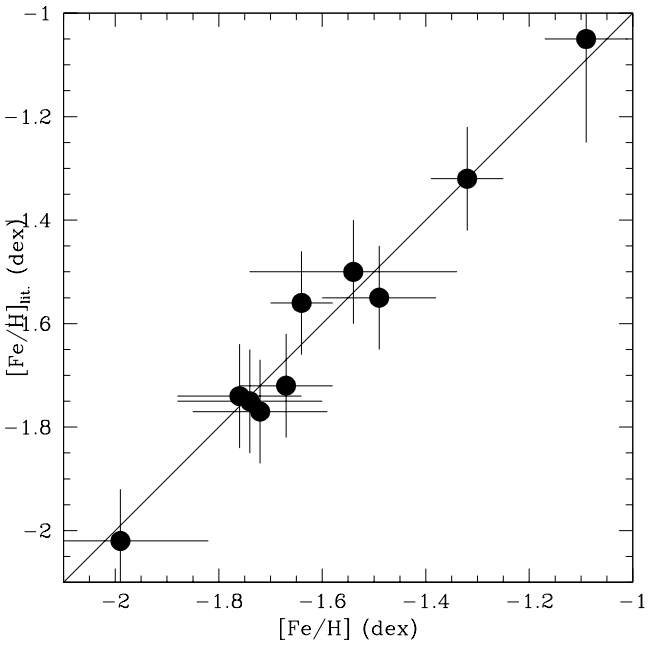

Figure 3. Relationship between our [Fe/H] values and those taken from the literature (see Table 2).

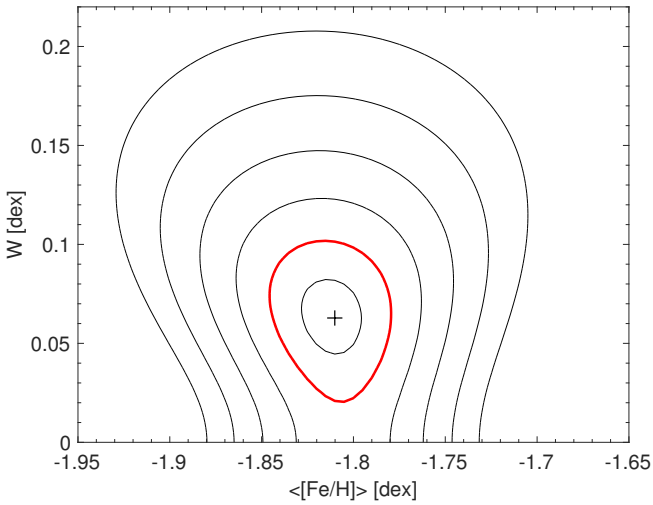

Figure 4. Likelihood distribution for the mean and dispersion of NGC 1786, the only GC in our sample that shows a non-zero intrinsic dispersion. Contours show confidence levels of 0.5–3σ with the 68% interval highlighted in red.

Martell, S. L., & Grebel, E. K. 2010, A&A, 519, A14, doi: 10.1051/0004-6361/201014135

Milone, A. P., Bedin, L. R., Piotto, G., & Anderson, J. 2009, A&A, 497, 755

Mucciarelli, A., Origlia, L., & Ferraro, F. R. 2010, ApJ, 717, 277, doi: 10.1088/0004-637X/717/1/277

Mucciarelli, A., Origlia, L., Ferraro, F. R., & Pancino, E. 2009, ApJL, 695, L134, doi: 10.1088/0004-637X/695/2/L134

Ordoñez, A. J., & Sarajedini, A. 2015, AJ, 149, 201, doi: 10.1088/0004-6256/149/6/201

Osborn, W. 1971, The Observatory, 91, 223

Piatti, A. E., & Geisler, D. 2013, AJ, 145, 17, doi: 10.1088/0004-6256/145/1/17

Piatti, A. E., Geisler, D., Sarajedini, A., & Gallart, C. 2009, A&A, 501, 585, doi: 10.1051/0004-6361/200912223

Piatti, A. E., & Mackey, A. D. 2018, MNRAS, doi: 10.1093/mnras/sty1048

Pompéia, L., Hill, V., Spite, M., et al. 2008, A&A, 480, 379

Stetson, P. B., Davis, L. E., & Crabtree, D. R. 1990, in Astronomical Society of the Pacific Conference Series, Vol. 8, CCDs in astronomy, ed. G. H. Jacoby, 289–304

Suntzeff, N. B., Schommer, R. A., Olszewski, E. W., & Walker, A. R. 1992, AJ, 104, 1743, doi: 10.1086/116356

Van der Swaelmen, M., Hill, V., Primas, F., & Cole, A. A. 2013, A&A, 560, A44

Wagner-Kaiser, R., Mackey, D., Sarajedini, A., et al. 2018, MNRAS, 474, 4358, doi: 10.1093/mnras/stx3061

—. 2017, MNRAS, 471, 3347, doi: 10.1093/mnras/stx1702

Walker, M. G., Mateo, M., Olszewski, E. W., et al. 2006, AJ, 131, 2114, doi: 10.1086/500193